# Optical characterization and band offsets in ZnSe-$ZnS_xSe_{1-x}$ strained-layer superlattices

Khalid Shahzad* and Diego J. Olego
*Philips Laboratories, North American Philips Corporation, 345 Scarborough Road, Briarcliff Manor, New York 10510*

Chris G. Van de Walle
*IBM Research Division, Thomas J. Watson Research Center, P.O. Box 218, Yorktown Heights, New York 10598*
(Received 8 September 1987; revised manuscript received 19 October 1987)

Photoluminescence and excitation experiments were carried out to study effects of the strain and carrier confinement in ZnSe-$ZnS_xSe_{1-x}$ strained-layer superlattices (SLS's) grown by molecular-beam epitaxy on GaAs substrates. For the case where the total thickness of the SLS is very small (1000 Å), the structure grows pseudomorphically to the buffer layer. The ZnSe well layers are not strained and all the blue shift in the optical spectra is attributed to the carrier confinement effects only. At the other extreme, for the case of a SLS with very large total thickness ($\sim 4$ $\mu$m), we show that it can be treated as free-standing with ZnSe layers under biaxial compression and $ZnS_xSe_{1-x}$ layers under biaxial tension. In the cases of intermediate total thicknesses, we show that SLS's are not fully relaxed to their equilibrium states by measuring the strains directly in the ZnSe well layers. Empirical values for the band offsets are obtained from the analysis of the optical response as a function of the sample parameters. Theoretical calculations of the band offsets, based on the model solid approach, were also performed and are found to agree with the experimental observations to within 0.05 eV. They indicate that all possible ZnSe-$ZnS_xSe_{1-x}$ interfaces will exhibit a very small conduction-band offset.

## I. INTRODUCTION

With the advent of modern epitaxial growth techniques such as molecular-beam epitaxy (MBE), it has become possible to grow semiconductor superlattices and quantum well structures and tailor the band structures to achieve the desired properties and device applications. Strained-layer superlattices (SLS's) give an additional degree of freedom by allowing heteroepitaxial growth of lattice-mismatched systems without creating misfit dislocations.[1] The strain energy in these structures is taken up by the elastic deformation of the lattice. Wide-band-gap II-VI compound multilayer structures are eminently suitable for various optoelectronic devices covering from the visible to the ultraviolet spectral range. In particular, ZnSe-$ZnS_xSe_{1-x}$ SLS's are potentially useful for electron-beam-pumped blue lasers[2] for printing applications and various other optoelectronic devices including blue-light-emitting diodes and blue injection lasers [The band gaps of ZnSe and ZnS at 5 K are 2.83 eV (438.0 nm) and 3.84 eV (322.8 nm), respectively]. Recently, there has been a report of a ZnSe-ZnS SLS grown by low-pressure organometallic vapor phase epitaxy (LP OMVPE) in which the authors observed a very large blue shift for very thin wells.[3] (The room-temperature lattice constants of ZnSe and ZnS are given in Table I.) Although there had also been a report of the growth of a ZnSe-$ZnS_xSe_{1-x}$ SLS,[4] it was only recently that clear evidence of quantization effects was presented in this structure.[5]

In this work, we used low-temperature photoluminescence (PL) to study the effects of strain and quantum confinement on the band edges of both the well and barrier layers in ZnSe-$ZnS_xSe_{1-x}$ ($x < 0.30$) SLS's. We studied several superlattice structures ranging from $\sim 1000$ Å to $\sim 4$ $\mu$m *total* thickness. In the former case, we find that the SLS grows pseudomorphically to the ZnSe buffer layer, showing zero strain in the well layers, while in the latter case of the thick superlattice, the strain is shared between the well and the barrier layers governed by their relative thicknesses and elastic constants. We also studied the intermediate cases of the SLS, where we show that

TABLE I. Elastic constants, electron and heavy-hole masses, and lattice constants (300 K) for ZnSe and ZnS.

| | $C_{11}$ ($10^6$ kg cm$^{-2}$) | $C_{12}$ ($10^6$ kg cm$^{-2}$) | $m_e^*$ (units of $m_0$) | $m_{hh}^*$ (units of $m_0$) | Lattice constants (Å) |
|---|---|---|---|---|---|
| ZnSe | 0.826[a] | 0.498[a] | 0.17[b] | 0.60[b] | 5.6686 |
| ZnS | 1.067[c] | 0.666[c] | 0.27[d] | 0.49[d] | 5.4093 |

[a]Reference 19.
[b]Reference 21.
[c]Reference 20.
[d]Reference 22.

 

these structures have not fully reached their equilibrium, free-standing states. In these cases, we estimate the value of strain measured directly in the well by the Raman probe.

We also present theoretical results of the heterojunction band discontinuities in this strained-layer system, based on the theory by Van de Walle and Martin.[6] The calculated band offsets agree with experiment to within the theoretical error bar of 0.05 eV, and allow us to draw general conclusions about the lineups in this system. The paper is organized as follows. Section II discusses the experimental procedures employed; Secs. III and IV give the theoretical background to the strain and quantum confinement effects appropriate for the analysis of the present work. In Sec. V we present the experimental results by, in Sec. VI, theoretical derivation of the band offsets. Section VII presents a discussion of the work, and, finally, conclusions are given in Sec. VIII.

## II. EXPERIMENTAL PROCEDURE

All the superlattices were grown by MBE on [001]-oriented GaAs substrates at 350°C. The lattice mismatch between ZnSe and GaAs ($a_{GaAs}=5.6533$ Å) is 0.27% at room temperature. It has been shown that the strain due to this mismatch is almost fully relaxed by the time the ZnSe epilayer thickness is about 1 $\mu$m.[7] Therefore, for the present study, each SLS structure was grown on about a 1-$\mu$m-thick ZnSe buffer layer. The thicknesses of the well and barrier layers were kept well within their "critical thickness." This critical thickness basically corresponds to a limit between the strain-accommodated mismatch and the onset of misfit dislocation formation. Values of this parameter as a function of the sulfer composition and the corresponding lattice mismatch to ZnSe have been plotted in Fig. 1. These curves were computed using the expressions derived by Matthews and Blakeslee[8] and People and Bean[9] and with the Burgers vector of 4 Å and a Poisson's ratio of 0.38 and used in this work only to give a rough guideline to the order of magnitude of the epilayer thickness which may be grown without running into severe problems with misfit dislocations. In practice, our individual layer thicknesses were well below the critical layer thicknesses predicted by even the most pessimistic of the two models discussed above. Also, for the particular case of ZnSe on GaAs, which has 0.27% lattice mismatch, the critical layer thickness was determined by transmission electron microscopy (TEM) to be of the order of 1500 Å[7], contrasted with a predicted value of about 500 Å by the Matthews Blakeslee model, and about 2 $\mu$m by the People-Bean model. In the present case, the sulfur compositions of the barrier layers were inferred from Raman measurements of the longitudinal-optical phonons. The ZnSe-like phonons have a strong dependence on sulfur composition[10] and therefore they can be used to monitor it very accurately. The Raman shifts in the phonons of the ZnSe layers give a direct determinations of the biaxial strains. A complete Raman study goes beyond the scope of this paper and will be published elsewhere. In some samples, we were also able to detect PL signal from the ternary layers: the two sets of data

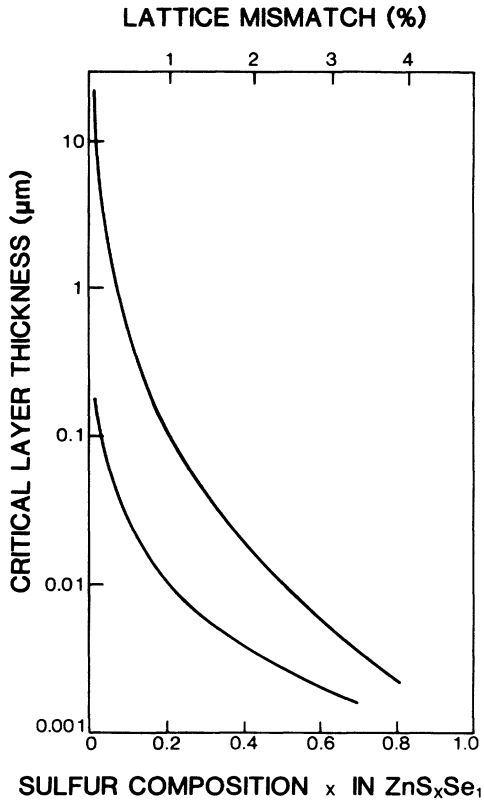


FIG. 1. Critical layer thickness as a function of sulfur composition $x$, for $ZnSe_xSe_{1-x}$ grown on a ZnSe substrate. The upper curve is computed using the expression from Ref. 9 while the lower one is from Ref. 8 using Burgers vector of 4 Å and a Poisson's ratio of 0.38.

were in excellent agreement with each other. The layer thicknesses were determined by TEM and ranged from 18 to 160 Å. The interfaces were also examined by TEM, which showed them to be smooth and regular with little or no evidence of misfit dislocations. With the exception of two samples (c and e in Table III), the *total* thickness of each of the superlattices studied here was of the order of 1 $\mu$m. Of the two samples noted above, one consisted of 801 epilayers of alternating ZnSe and $ZnS_xSe_{1-x}$ ($x\sim0.15$) with each layer being 50 Å thick, i.e., a total superlattice thickness of about 4 $\mu$m (sample e), while the other had a total thickness of the order of 1000 Å. The PL spectra were measured with the samples at 5 K and using 363.8–351.1-nm excitation lines from an Ar-ion laser. The signal was dispersed with an $f7.8$, 0.85 m Spex double monochromator and detected with an RCA Erma III photomultiplier tube and lock-in amplifier.

## III. EFFECT OF STRAIN ON THE BAND EDGES

If the total thickness of a strained-layer superlattice is substantially larger than a certain critical thickness, then we would expect the superlattice to relax to its equilibrium lattice constant rather than maintain the lattice constant of the buffer layer. In this free-standing case, the heterolayers would assume a new equilibrium lattice constant causing an in-plane extension of the layer with the

smaller lattice constant and compression of the layer with the larger lattice constant. On the contrary, if the superlattice has a total thickness much smaller than its critical thickness, then we would expect it to assume almost the same lattice constant as the buffer layer, i.e., relaxation is expected to be negligibly small. For the particular case of a free-standing ZnSe-$ZnS_xSe_{1-x}$ SLS, the equilibrium in-plane lattice constant of the superlattice is given by[1]

$$a^{\parallel}= a_{\mathrm{ZnSe}}\left[1-\frac{f G_{\mathrm{ZnS_xSe_{1-x}}} d_{\mathrm{ZnS_xSe_{1-x}}}}{G_{\mathrm{ZnSe}} d_{\mathrm{ZnSe}}+G_{\mathrm{ZnS_xSe_{1-x}}} d_{\mathrm{ZnS_xSe_{1-x}}}}\right], \quad (1)$$

where $f$ is lattice mismatch of ZnSe with respect to $ZnS_xSe_{1-x}$ given by $f=(a_{\mathrm{ZnSe}}-a_{\mathrm{ZnS_xSe_{1-x}}})/a_{\mathrm{ZnS_xSe_{1-x}}}$, $G_i$ are shear moduli given by

$$G_i=2\left[C_{11}^i+C_{12}^i-\frac{2(C_{12}^i)^2}{C_{11}^i}\right], \quad (2)$$

$C_{ij}$'s are the elastic stiffness constants, $d_i$'s are the layer thicknesses, and $a_i$'s are the lattice constants (Table I). If we define $z\|[001]$ (i.e., along the growth direction), then the strain tensors $\epsilon_{ij}$, corresponding to the ZnSe layers, are given by

$$\epsilon_{xx}=\epsilon_{yy}=\left[\frac{a_{\parallel}-a_{\mathrm{ZnSe}}}{a_{\mathrm{ZnSe}}}\right], \quad (3a)$$

$$\epsilon_{zz}=-\frac{2C_{12}}{C_{11}}\epsilon_{xx}, \quad (3b)$$

$$\epsilon_{xy}=\epsilon_{yx}=\epsilon_{zx}=0. \quad (3c)$$

For a zinc-blende-type material, the valence bands at $k=0$ consist of a fourfold $P_{3/2}$ multiplet ($J=\frac{3}{2}$; $m_J=\pm\frac{3}{2},\pm\frac{1}{2}$) and a twofold $P_{1/2}$ multiplet ($J=\frac{1}{2}$; $M_J=\pm\frac{1}{2}$). For the case of biaxial in-plane compression, the $P_{3/2}$ valence band splits because of lowering in the symmetry from $T_d$ to $D_{2d}$. In addition, the hydrostatic component of the stress shifts the center of gravity of $P_{3/2}$ and $P_{1/2}$ multiplets relative to the bottom of the lowest conduction band and may also influence the relative lineups and thus the band discontinuities between the two materials. The fourfold degenerate $P_{3/2}$ splits into a doubly degenerate $U_1$ band and a $U_2$ band (Fig. 2). The spin-orbit split-off band is given as $U_3$. Pikus and Bir[11] have shown that the orbital strain Hamiltonian for a given band at $k=0$ can be written as

$$H_\epsilon=-a(\epsilon_{xx}+\epsilon_{yy}+\epsilon_{zz})-3b[(L_x^2-\tfrac{1}{3}L^2)\epsilon_{xx}+\text{c.p.}] -\sqrt{3}d[(L_x,L_y)\epsilon_{xy}+\text{c.p.}], \quad (4)$$

where $\epsilon_{ij}$ denotes the components of the strain tensor, $L$ the angular momentum operator, c.p. denotes the cyclic permutation with respect to the indices $x$, $y$, and $z$, and $(L_x,L_y)$ indicate the symmetrized product: $\frac{1}{2}(L_xL_y+L_yL_x)$. The parameter $a$ is the hydrostatic deformation potential. The quantities $b$ and $d$ are the shear deformation potentials appropriate to the strain of tetragonal and rhombohedral symmetries, respectively. Since we can experimentally measure only the energy difference between two bands, it is only possible to determine the relative hydrostatic pressure coefficient between the conduction band and the valence band. From the theoretical point of view, however, it is useful to define the hydrostatic deformation potentials $a_v$ and $a_c$ for (the center of gravity of) the valence and conduction bands, respectively. This will enable us to predict the positions of the bands in a strained structure. We have, of course, $a=(a_c-a_v)$. Notice that the direct conduction-band minimum at $\Gamma$ is only subject to the hydrostatic component of the strain, and not influenced by uniaxial components.

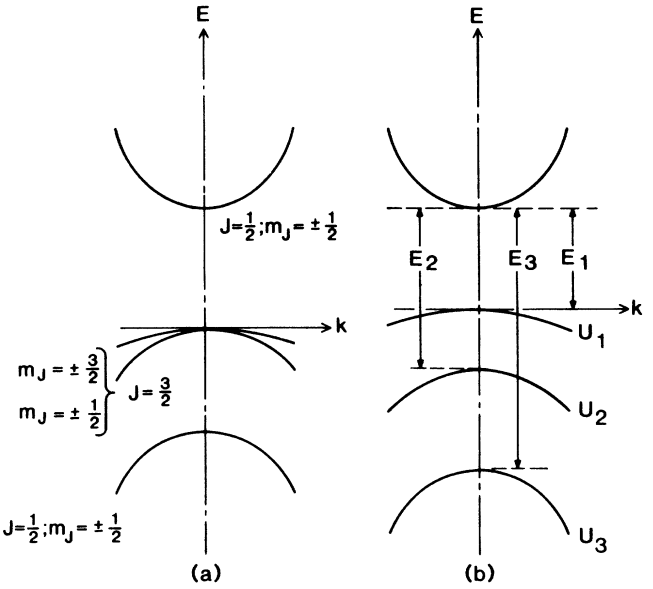


FIG. 2. Schematic representation of the valence bands and the lowest conduction band (a) unstrained and (b) strained due to biaxial compressive stress, in zinc-blende-type material near $k=0$.

In the case of $z\|[001]$, the strain Hamiltonian becomes

$$H_\epsilon=-2a\left[\frac{C_{11}-C_{12}}{C_{11}}\right]\epsilon_{xx} +3b\left[\frac{C_{11}+2C_{12}}{C_{11}}\right]\epsilon_{xx}(L_z^2-\tfrac{1}{3}L^2), \quad (5)$$

where the first term represents the shift of the center of gravity of $P_{3/2}$ and the second term describes the splitting of $P_{3/2}$ due to tetragonal distortion. The eigenvalues of the strain Hamiltonian can be calculated by using the unperturbed wave functions of the valence and conduction bands in a zinc-blende-type material. The calculated energy difference between the conduction and valence bands at $k=0$ is given by[12]

$$\Delta E_1=E_H+E_U, \quad (6a)$$

$$\Delta E_2=E_H+\tfrac{1}{2}(\Lambda-E_U)-\tfrac{1}{2}(9E_U^2+2\Lambda E_U+\Lambda^2)^{1/2}, \quad (6b)$$

$$\Delta E_3=E_H+\tfrac{1}{2}(\Lambda-E_U)+\tfrac{1}{2}(9E_U^2+2\Lambda E_U+\Lambda^2)^{1/2}, \quad (6c)$$

where

$$E_H = 2a\left[\frac{C_{11}-C_{12}}{C_{11}}\right]\epsilon_{xx} ,$$

$$E_U = -b\left[\frac{C_{11}+2C_{12}}{C_{11}}\right]\epsilon_{xx} ,$$

and $\Lambda$ is the spin-orbit splitting.

The values of the various deformation potentials can be derived from first-principles calculations, using local-density-functional theory and *ab initio* pseudopotentials, as described in Ref. 6. Calculated values of the hydrostatic and uniaxial deformation potentials $a_{\text{theor}}$ and $b_{\text{theor}}$ for ZnSe and ZnS are listed in Table II. For comparison, we also list experimental values of $a_{\text{expt}}$ and $b_{\text{expt}}$: the former were obtained from experimental data on the hydrostatic pressure coefficient of the lowest-energy gap $\partial E/\partial P$, using the relation $a = -\frac{1}{3}(C_{11}+2C_{12})\partial E/\partial P$. Values of deformation potentials, elastic constants, and spin-orbit splittings for alloys can be obtained by interpolating linearly between the pure binary materials. As an example of the expected effects of the strain, before quantum confinement is considered, Fig. 3 shows the uniaxial splittings (using the experimental values of the deformation potentials listed in Table II) of the valence-band edge of ZnSe in a free-standing SLS of equal well and barrier thicknesses, grown on [001]-oriented substrates. Note that the $U_1$ becomes the highest-lying valence-band edge in ZnSe which moves up in energy as the sulfur composition $x$ increases while $U_2$ moves down in energy. These bands move in the opposite direction in the case of $ZnS_xSe_{1-x}$ which is under biaxial tension. Note that although the shift of $U_1$ is linear in $\epsilon_{xx}$, it is not linear as a function of alloy composition. The anticrossing of $U_2$ and $U_3$ is due to the interaction between the states with the same magnetic quantum number (i.e., $m_J = \pm\frac{1}{2}$). The total shift of the valence-band edges with respect to the conduction band in the individual materials is shown in Fig. 4. It can be seen that the top of the valence band in the ZnSe layer will be given by $m_J = \pm\frac{3}{2}$ while that in $ZnS_xSe_{1-x}$ will be given by $m_J = \pm\frac{1}{2}$. Therefore, the band gap of ZnSe *increases* while that of $ZnS_xSe_{1-x}$ *decreases* (at a faster rate) as the composition $x$ increases. The shifts in the band edges given in Fig. 4 apply to any thickness of the well and barrier so long as they are equal (but, of course, below their critical layer thicknesses) since it is clear from Eq. (1) that the effective strain in each of the layers is a function of only the *relative* thicknesses of the layers and not their absolute thicknesses, assuming their elastic properties are not very different from each other.

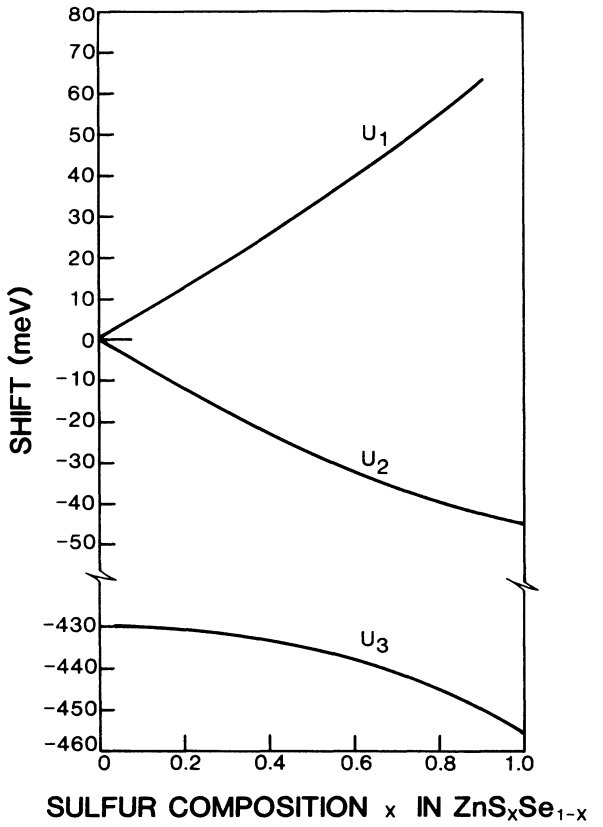


FIG. 3. Splittings of the $J=\frac{3}{2}$ and $J=\frac{1}{2}$ valence-band edges of the ZnSe well with equal $ZnS_xSe_{1-x}$ barrier thickness, due to tetragonal distortion, as a function of the alloy composition $x$, grown on [001]-oriented substrates. Note that $U_1$ is slightly nonlinear in alloy composition and that the states $U_2$ and $U_3$ curve away from each other due to the interaction between the states with the same magnetic quantum number ($m_J=\pm\frac{1}{2}$). These curves were calculated using the experimental values of the deformation potentials listed in Table II and assuming a free-standing case.

TABLE II. Spin-orbit splitting ($\Lambda_0$), direct energy gap $E_g$ (4 K), and theoretical and experimental hydrostatic deformation potentials ($a_{\text{theor}}$ and $a_{\text{expt}}$), theoretical and experimental uniaxial deformation potentials ($b_{\text{theor}}$ and $b_{\text{expt}}$) of ZnSe and ZnS. Also given are "absolute" energy positions (within the "model solid" approach) of the center of gravity of the valence bands ($E_{v,\text{av}}$) and conduction band ($E_c$), and hydrostatic deformation potentials of (the center of gravity of) the valence band ($a_v$) and the conduction band ($a_c$) of ZnSe and ZnS. All units are in eV.

| | $\Lambda_0$ | $E_g$ | $a_{\text{theor}}$ | $a_{\text{expt}}$ | $b_{\text{theor}}$ | $b_{\text{expt}}$ | $E_{v,\text{av}}$ | $E_c$ | $a_v$ | $a_c$ |
|---|---|---|---|---|---|---|---|---|---|---|
| ZnSe | 0.43[a] | 2.83 | −5.82 | −5.40[b] | −1.2 | −1.2[c] | −8.37 | −5.4 | 1.65 | −4.17 |
| ZnS | 0.07[a] | 3.84 | −6.4 | −4.56 | −1.25 | −0.75[c] | −9.15 | −5.29 | 2.31 | −4.09 |

[a]Reference 23.
[b]Reference 24.
[c]Reference 25.

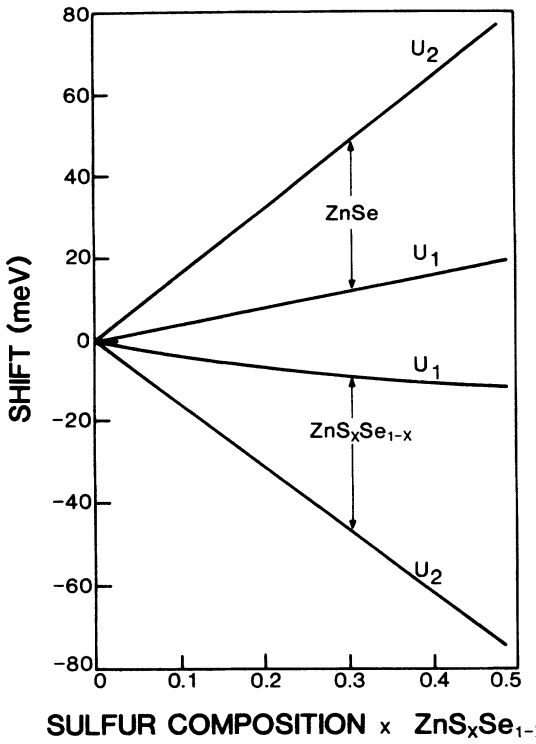


FIG. 4. Total shifts in the band edges of equal thicknesses of ZnSe and $ZnS_xSe_{1-x}$ strained-layer free-standing superlattices as a function of the alloy composition. Positive shift means that the tops of the valence-band edges are increasing in separation from the bottom of the lowest conduction band as is the case for the ZnSe layers. In this case, the band gap will be formed between the bottom of the conduction band and the $U_1$ valence band while in the case of $ZnS_xSe_{1-x}$, which is under biaxial tension, the band gap will be formed by the $U_2$ valence band and decreases as a function of the alloy composition. These curves were calculated using the experimental data given in Tables I and II.

## IV. QUANTUM CONFINEMENT EFFECTS

In addition to the strain-induced renormalization of the energy bands, electron and hole confinement also causes the transition energies to move to higher energies. This blue shift is a function of the band offsets and the effective masses of the carriers involved. The confinement energies are calculated by solving numerically the dispersion relations[13]

$$\cos(kl)=\cos(k_z l_z)\cosh(k_b l_b)+\frac{1}{2}\left[x-\frac{1}{x}\right]\sin(k_z l_z)\sinh(k_b l_b)\ , \tag{7}$$

where $l$ is the superlattice period and $l_z$ and $l_b$ are well and barrier widths and

$$x=\left[\frac{k_b}{k_z}\frac{m_z}{m_b}\right]\ ,$$

$$hk_z=(2m_zE)^{1/2}\ ,\quad hk_b=[2m_b(V-E)]^{1/2}\ ,$$

where $m_z$ and $m_b$ are the effective masses in the well and barrier layers and $V$ is the potential barrier height corresponding to, in our case, valence- or conduction-band offsets. Note that the above equation is not identical to the usual Kronig-Penney result since $x$ is an explicit function of $m_z$ and $m_b$. The effective masses of electrons and holes in ZnSe and ZnS are given in Table I. We have, again, taken linearly interpolated values for the $ZnS_xSe_{1-x}$ alloy.

## V. EXPERIMENTAL RESULTS

Figure 5(a) shows typical 5-K PL spectra in the excitonic region for three of the ZnSe-$ZnS_xSe_{1-x}$ SLS's. For comparison purposes, we have also included a spectrum from a 4.9-$\mu$m-thick ZnSe epilayer grown on a [001] GaAs substrate. The band edge PL from the 4.9-$\mu$m epilayer consists of free exciton (polariton) emission as well as impurity-bound excitons. The ground-state free exciton[14] at 2.8033 eV is labeled as $E_{GX}^{n=1}$. The most prominent feature is the peak labeled as $I_{2o}^{Ga}$ at 2.7949 eV with a full width at half maximum (FWHM) of $\sim$0.7 meV. We believe that this peak is due to the ground-state recombination of the exciton bound to the neutral Ga donor at the Zn site. The most direct evidence for this assignment comes from the two-electron (2e) satellites related to the Ga donor which can be seen very clearly in this sample at lower energies than $I_{2o}^{Ga}$ (not shown in the figure). In addition, we have also observed in this particular sample two transitions at 2.7913 and 2.7903 eV. The former is tentatively assigned to the Li acceptor bound exciton, $I_1^{Li}$, while the chemical origin of the latter (labeled as $I_1^X$) is not yet established. These results strongly support the idea that Ga does diffuse into the epilayer during the growth process, even in the case of such a thick layer.

The emission spectra of the quantum wells with good interfaces (as shown by transmission electron microscopy) demonstrate the contribution due to the free exciton recombination peak at higher energy and a second lower-energy peak attributed to bound excitons [Fig. 5(a)]. The free exciton intensity relative to bound excitons has increased tremendously even at very low temperatures where bound exciton and impurity-related processes dominate for the bulk ZnSe.[5] Both of the peaks are relatively broad ($\sim$3 meV) as compared to the case of the thick layer. Nevertheless, we want to emphasize that these linewidths are much narrower than those of typical III-V strained-layer superlattices.[15] The energy separation between the two peaks remains constant at about 6 meV as the superlattice period is changed. We also carried out PL excitation measurements as shown in Fig. 5(b). For the case of sample g, we were able to detect the ground-state free exciton (labeled as $e_{1h}$) and the first excited state due to a transition between the $n=1$ electron to light-hole subbands ($e_{1l}$). The energy positions of $e_{1h}$ and $e_{1l}$ agree very well with those calculated based on the band offsets given in Table V and a strain splitting between heavy- and light-hole bands of 8 meV. In the case of sample e, however, we could observe only the ground state $e_{1h}$ transition due to the unavailability of useful pump intensities, in the deep blue region of the spectrum,

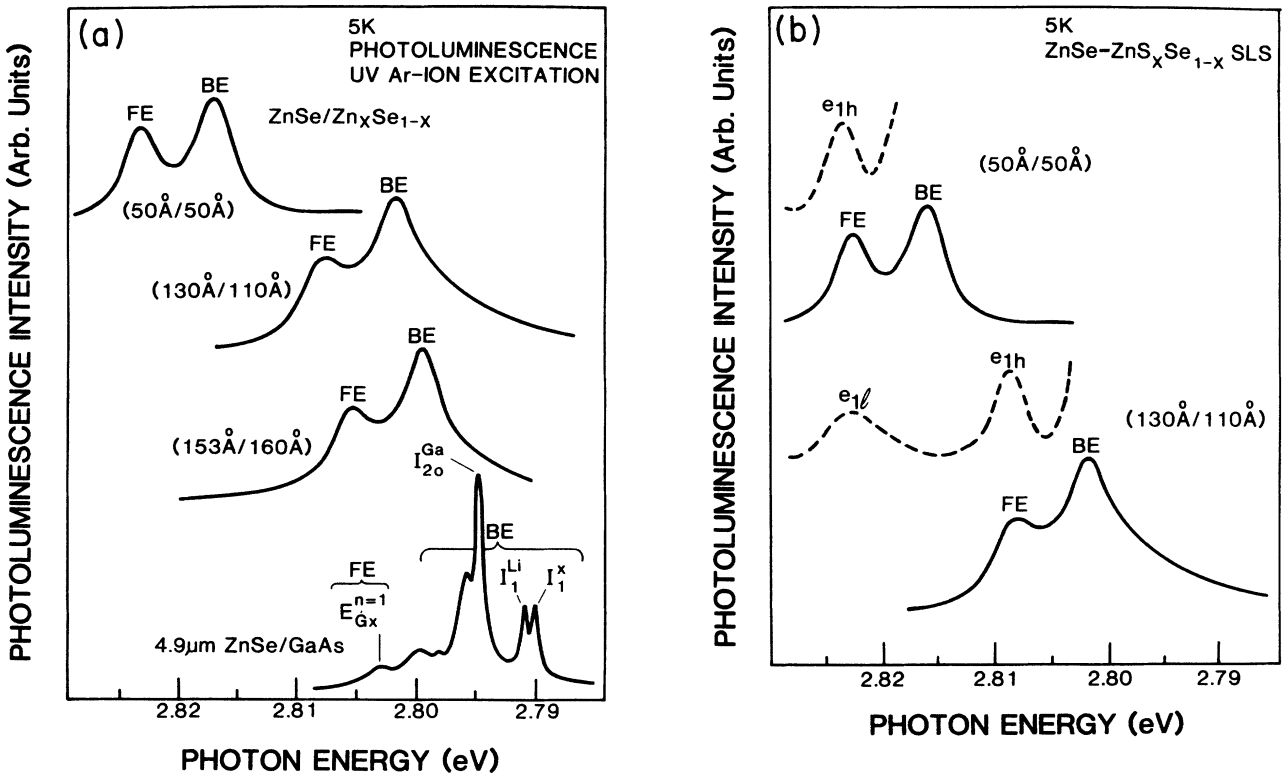


FIG. 5. (a) Low-temperature photoluminescence spectra of three ZnSe-$ZnS_xSe_{1-x}$ strained-layer superlattices with well widths of 50, 130, and 153 Å each showing free exciton (FE) and bound exciton (BE) transitions. For comparison, we also show a 4.9-$\mu$m ZnSe/GaAs showing very narrow and sharp bound exciton peaks (see also Fig. 6). Note a very clear shift of the exciton peaks to higher energies as the well width decreases. (b) Photoluminescence (solid) and excitation (dashed) spectra at 5 K for two of the strained-layer superlattices of ZnSe-$ZnS_xSe_{1-x}$ with well widths of 130 and 50 Å. For the excitation case, the detector was set at 2.801 eV for the former case and at 2.816 eV for the latter case. $e_{1h}$ and $e_{1l}$ indicate the calculated $n=1$ electron to heavy- and light-hole subband-related transitions, respectively.

from the dye laser. Nevertheless, we find that our designation of the free exciton peaks on PL are consistent with excitation measurements which show them to be due to ground-state electron to heavy-hole subband-related transitions. Figure 6(a) shows the ratio $R$ of the lower-energy peak (BE) intensity to higher-energy peak (FE) intensity as a function of the temperature for 50-Å–50-Å superlattice. We see clearly that as the temperature is increased above 5 K, the lower-energy peak becomes weak compared with the higher-energy peak and almost disappears at around 100 K. Also, from the incident intensity dependence of the two peaks [Fig. 6(b)], we see that, initially, the higher-energy peak has a slightly stronger dependence on the pump intensity. These observations lead us to conclude that the higher-energy peak is consistent with the free exciton transition as assumed earlier and the lower-energy peak is due to impurity-related excitons; most probably, donor related. Comparing the free exciton energy position in the cases of the superlattices with that of the thick epilayer, we see that there is a clear shift of the excitons to higher energies in the case of superlattices (see Fig. 5). This blue shift is caused by a combination of strain effects due to the lattice mismatch discussed above and also due to the quantum confinement of the electrons and holes. The contributions of the strain-induced effects to the experimental shifts were accounted for in the following manner. The sulfur composition of the ternary barrier layers in our superlattices was different from sample to sample. This composition for each sample was determined by Raman and PL measurements as described earlier and is listed in Table III. Furthermore, we found that the strains measured by Raman ($\epsilon_{xx}^{R}$) directly in ZnSe wells were quite often much smaller (by a factor of almost 2) than one would estimate based on the sulfur composition of the ternary layers ($\epsilon_{xx}^{X}$) and the ensuing lattice mismatch, *assuming* that the superlattice is free-standing (Table III). This suggests that, in these cases, the superlattices have not reached their equilibrium, free-standing state, despite the fact that they are of the order of 1 $\mu$m in total thickness. If one assumes a free-standing case for all the samples thicker than 1 $\mu$m then $\Delta_{\text{strain}}$ becomes larger than the measured shifts. Therefore, for the purpose of calculating the strain-induced shifts in the ZnSe band gap and the band offsets, as discussed later, we used the directly measured values of these strains, as given by Raman measurements. The components of the shifts in the band gaps due to these strains ($\Delta_{\text{strain}}$) are listed in Table IV.

In order to calculate the quantum confinement energies, we require the values of the conduction- and

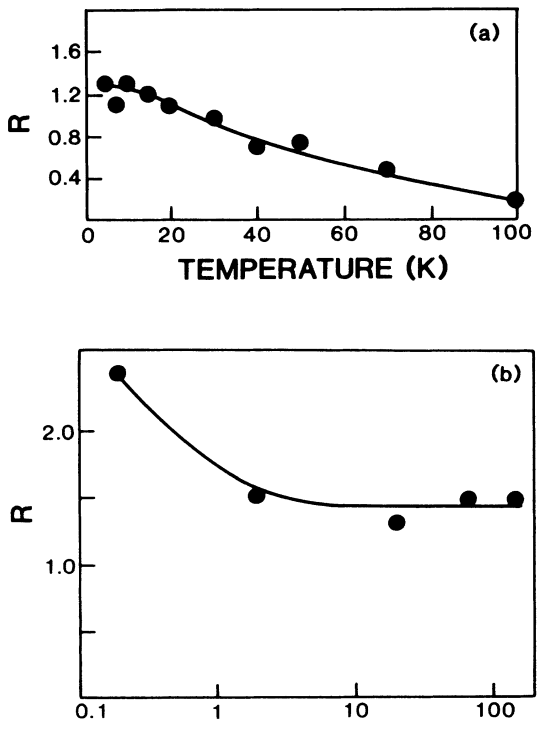


FIG. 6. (a) Ratio of the bound exciton to the free exciton intensities ($R$) as a function of the temperature of the sample e (50-Å–50-Å) strained-layer superlattice; and (b) ratio $R$ as a function of incident pump power intensity for the same sample.

valence-band offsets for each of the SLS's we studied. We arrive at the values of the band offsets by an empirical fit to the difference $(\Delta_{\text{total}}^{\text{expt}} - \Delta_{\text{strain}})$ with Eq. (7) and by using the band offset $V$ as an adjustable parameter. As an example, in the case of sample e (50-Å–50-Å) SLS with $x \sim 0.19$, which is assumed to be free-standing based on the fact that the calculated and measured values of the strain agree with each other (see Table III), the shift in the band gap of ZnSe wells due to the strain alone is calculated to be about 5 meV to higher energies. The remaining shift of 15 meV is attributed to carrier confinement effects. We obtain the best fit to the total experimental shift if we assume the conduction-band discontinuity $\Delta E_c$ of about $-3$ meV (the negative sign indicates that the band is lower in ZnSe; see the inset to Fig. 7) and a corresponding valence-band discontinuity of $\Delta E_v$ of about 109 meV. This gives an electron confinement energy of $\sim 2$ meV and a heavy-hole confinement energy of $\sim 15$ meV, thus giving a total shift of $\sim 22$ meV. The ground-state electronic confinement energy is a much stronger function of the barrier height in the small barrier height region (of the order of 20 meV) whereas in the case of the heavy holes, the confinement energies for the larger barrier heights (of the order of 100 meV) do not change very rapidly, by comparison. For example, for the case of a superlattice with equal well and barrier widths of 50 Å each, if $\Delta E_c$ is increased from $-3$ to $-50$ meV, then the confinement energy of the electron increases from 2 to 20 meV, i.e., by a factor of 10. However, at the same time, $\Delta E_v$ decreases from 109 to 62 meV, but the heavy-hole confinement energy decreases from 15 to only 12 meV. Therefore, if $\Delta E_c$ was substantially larger than $-3$ meV for sample e, then this would have large observable effects on the superlattice band gap. We find, in general, that the conduction-band offsets for all the compositions studied are very small. The so determined $\Delta E_c$ and $\Delta E_v$ are listed in Table V.

TABLE III. Well ($L_w$) and barrier ($L_b$) widths (Å) of the superlattices studied. $x$ is the sulfer composition in the ternary $ZnS_xSe_{1-x}$ layers as measured by Raman and photoluminescence techniques. $\epsilon_{xx}^X$ gives the percent strain estimated from the sulfer composition assuming the superlattices are free-standing, while $\epsilon_{xx}^R$ gives the strain values computed directly in the ZnSe layers using Raman experiments (negative values of the strain imply a biaxial compression for ZnSe layers). In the case of sample a, the measured strain by Raman is $\sim 0.1\%$, but we believe that this value is lower than the actual value of the strain due to phonon confinement effects in such a narrow well structure. The value of 0.3% is estimated based on the strain configurations of other samples studied which have similar total thicknesses. (NA indicates data were not available.)

| Sample | $L_w$ | $L_b$ | $x$ | $\epsilon_{xx}^X$ | $\epsilon_{xx}^R$ |
|---|---|---|---|---|---|
| a | 18 | 24 | 0.25 | −0.60 | −0.3 |
| b | 30 | 128 | 0.26 | −1.00 | −0.5 |
| c | 40 | 43 | 0.14 | −0.30 | 0 |
| d | 46 | 49 | 0.2 | −0.50 | −0.2 |
| e | 50 | 50 | 0.19 | −0.40 | −0.4 |
| f | 63 | 63 | 0.11 | −0.26 | NA |
| g | 130 | 110 | 0.07 | −0.16 | NA |
| h | 153 | 160 | 0.03 | −0.07 | NA |

## VI. THEORETICAL DETERMINATION OF BAND OFFSETS

The treatment in Sec. III shows that the *relative* positions of valence and conduction bands in a single semi-

TABLE IV. Strain-related shifts in the ZnSe band gap ($\Delta_{\text{strain}}$), ground-state heavy-hole ($E_{1\text{hh}}$) and electron confinement energies ($E_{1e}$). $\Delta_{\text{total}}^{\text{theor}}$ and $\Delta_{\text{total}}^{\text{expt}}$ are calculated and experimental shifts in the band gap (all units are in meV). The strain-related shifts are calculated based on the strains measured directly in the ZnSe layers (see Table III). For sample a, the values are calculated using $-0.3\%$ strain. Note in the case of sample c that there is zero strain in ZnSe wells since its total thickness is only of the order of 1000 Å.

| Sample | $\Delta_{\text{strain}}$ | $E_{1\text{hh}}$ | $E_{1e}$ | $\Delta_{\text{total}}^{\text{theor}}$ | $\Delta_{\text{total}}^{\text{expt}}$ |
|---|---|---|---|---|---|
| a | 5 | 44 | 5 | 54 | 45 |
| b | 8 | 30 | 4 | 42 | 46 |
| c | 0 | 19 | 3 | 22 | 22 |
| d | 4 | 15 | 2 | 21 | 22 |
| e | 5 | 15 | 2 | 22 | 20 |
| f | 4 | 10 | 2 | 16 | 16 |
| g | ~2 | 3 | 1 | 6 | 5 |
| h | 1 | 2 | 1 | 4 | 3 |

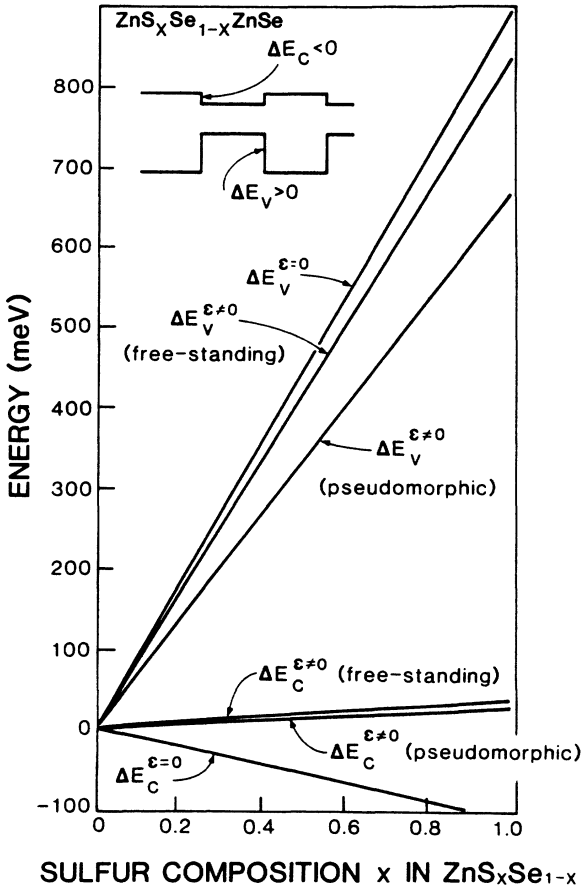


FIG. 7. Theoretical band offsets for the cases where the strain effects are neglected ($\Delta E_c^{\epsilon=0}$ and $\Delta E_v^{\epsilon=0}$), and the cases where the strain effects have been taken into account for a free-standing (thick) and a pseudomorphic (to ZnSe buffer layer) ZnSe-$ZnS_xSe_{1-x}$ strained-layer superlattice with equal well and barrier layer thicknesses grown on a ZnSe buffer layer. The inset shows the sign convention for the band alignment adopted here. Positive $\Delta E$ means the band is *higher* in ZnSe.

conductor can be completely described with the deformation potentials $a$ and $b$ (and, in a general case, $d$, which describes the uniaxial splitting under [111] strain [Eq. (4)]). To describe the band offsets at a heterojunction, however, one also requires information on the lineup of the band structures of the individual semiconductors. This information can be expressed as the discontinuity in the center of gravity of the valence band across the heterojunction. This center of gravity, which we denote as $E_{v,\mathrm{av}}$, is calculated as the weighted average over the valence bands at the zone center, $\Gamma$, which are split by uniaxial strain and spin-orbit effects. The theoretical derivation of the lineups, in principle, requires a full-fledged first-principles self-consistent interface calculation. Van de Walle and Martin have performed such calculations on a wide variety of lattice-matched and strained-layered heterojunctions.[6,16] More importantly, they were able to show that reasonable predictions for the offsets can be obtained by using information from *bulk* calculations alone, in the so-called *model solid* approach. Especially in the case of strained-layered structures, in which it would be impossible to repeat the full interface calculations for each desired strain configuration, and for which no other theory exists to date, the model offers a fast and reliable[17] way of deriving the band discontinuities. It should be emphasized that the theoretical results obtained with the model solid approach are based purely on first principles, and do not contain any fitting to experimental quantities. Based on examination of results for a large number of interfaces, the accuracy of the values for valence-band offsets between pure materials has been estimated to be 0.2 eV.[16] The error bar will be significantly smaller for the cases considered here, which consist of ZnSe/$ZnS_xSe_{1-x}$ interfaces with only a small fraction of ZnS in the alloy.

TABLE V. Theoretical and empirical values of the conduction-band offsets ($\Delta E_c^{\mathrm{theor}}$ and $\Delta E_c^{\mathrm{expt}}$) and valence-band offsets ($\Delta E_v^{\mathrm{theor}}$ and $\Delta E_v^{\mathrm{expt}}$) for various superlattices detailed in Table IV. Although the theoretically predicted values have an uncertainty of the order of $\sim 0.05$ eV, it is important to note that the *trends* between the experimental and theoretical values are correctly predicted. For the case of the conduction-band offsets, since the calculated values are much smaller than the error bars, it clearly shows that these offsets are very small, in agreement with the experimental observations and too small to differentiate between a type-I or a type-II lineup. The negative values of the conduction-band offsets in our notation indicate a type-I lineup. All units are in meV. (NA indicates data were not available.)

| Sample | $\Delta E_v^{\mathrm{theor}}$ | $\Delta E_v^{\mathrm{expt}}$ | $\Delta E_c^{\mathrm{theor}}$ | $\Delta E_c^{\mathrm{expt}}$ |
|---|---|---|---|---|
| a | 103 | NA | 5 | NA |
| b | 128 | 117 | 6 | −5 |
| c | 100 | 90 | 6 | −4 |
| d | 84 | 77 | 4 | −3 |
| e | 118 | 109 | 6 | −3 |
| f | 93 | 84 | 5 | −4 |
| g | 59 | 54 | 3 | −2 |
| h | 25 | 23 | 1 | −1 |

The model solid theory allows us to express the energies $E_{v,\mathrm{av}}$ on an absolute energy scale, and thus derive the band discontinuities by using $\Delta E_{v,\mathrm{av}}$ to line up the calculated band structures of two semiconductors. The relation

$$E_{v,\mathrm{av}} = E_{v,\mathrm{av}_0} + a_v \frac{\Delta V}{V} \tag{8}$$

expresses $E_{v,\mathrm{av}}$ in terms of its value in the unstrained material (i.e., at zero pressure, in its equilibrium volume), the hydrostatic deformation potential of the valence band, $a_v$, and the fractional volume change $\Delta V/V = \mathrm{Tr}(\epsilon) = \epsilon_{xx} + \epsilon_{yy} + \epsilon_{zz}$. The atomic calculations needed to derive the model solid values were performed with the configurations $s^{1.02}p^{0.98}$ for the cation, and $s^{1.86}p^{4.14}$ for the anion; bulk calculations were performed with an 18-Ry energy cutoff. This leads to the values listed in Table II. We should stress that these "absolute" values for $\Delta E_{v,\mathrm{av}}$ do not carry any meaning by themselves (and should certainly not be related to the ionization potential), but are only meaningful relative to similar quan-

tities in other semiconductors. In particular, for the II-VI compounds under study here, we have carried out all calculations with pseudopotentials which treat the $3d$ electrons of Zn as core electrons; this is a valid approximation since the effects due to the $d$ electrons are very similar in ZnS and ZnSe, and thus will cancel when looking at differences. The present values should *not* be used, however, to establish lineups between these materials and other, less similar, semiconductors. In Table II, we also give the positions of the conduction bands on the absolute energy scale. These have been derived by taking our calculated value for the valence band [a ground-state property, reliably predicted within the local-density approximation (LDA)], and adding to it the experimental band gap (from Table II). To derive the value of $E_c$ in a strained structure, we use

$$E_c = E_{c0} + a_c \frac{\Delta V}{V} . \tag{9}$$

From the values in Table II, we see that the conduction-band offset between ZnSe and ZnS, without taking any strain effects into account, is $\Delta E_c = -0.11$ eV (lower in ZnSe). This is comparable to a value of $-0.16$ eV obtained by Harrison's theory;[18] however, Harrison offers no prescription for including the strain effects, which we will show to be quite important.

The theoretical values listed in Table II, together with a knowledge of the strain configuration of the system, enables us to calculate all the band positions at a strained-layer interface, and derive the band discontinuities. As an example, we consider a strained layer of pure ZnS, deposited on a ZnSe substrate. The ZnSe is then unstrained, and the strains in ZnS can be derived from Eqs. (1)–(3); the splitting of the valence band is given by Eqs. (6). This leads to the following results: $\Delta E_{v,\mathrm{av}} = 0.70$ eV; $\Delta E_v = 0.58$ eV; $\Delta E_c = 0.03$ eV. In all cases, a positive value of the discontinuity corresponds to an upward step in going from ZnS to ZnSe (see inset of Fig. 7). Notice that the conduction-band discontinuity is small; this will be a more general result, as is discussed below.

## VII. DISCUSSION

We calculate the lineup for a ZnSe-$ZnS_xSe_{1-x}$ superlattice with equal layer thicknesses (Fig. 7). Band offset values for alloy compositions are all obtained using linear interpolation between the appropriate values for the pure materials.[6] For a sufficiently thin superlattice on a ZnSe substrate, the in-plane lattice constant $a^{\parallel}$ is determined by the substrate, and only the alloy layers are strained. This leads to the following lineups for $x = 0.25$, as an example: $\Delta E_{v,\mathrm{av}} = 0.18$ eV; $\Delta E_v = 0.17$ eV; $\Delta E_c = 0.01$ eV. In the case of a free-standing superlattice, the strain is distributed over both ZnSe and the alloy layers, and leads to $\Delta E_{v,\mathrm{av}} = 0.18$ eV; $\Delta E_v = 0.21$ eV; $\Delta E_c = 0.01$ eV. Notice that the change in lineups occurs mainly in the valence band, which is subject to the uniaxial strain splittings. The center of gravity of the valence band, $E_{v,\mathrm{av}}$, and the nondegenerate conduction band are only influenced by hydrostatic strain components, which have much smaller effects than the uniaxial splittings.

We have calculated the band offsets for all the samples with various well and barrier thicknesses, alloy compositions, and strain configurations in ZnSe layers. These values, along with the corresponding empirical values, are listed in Table V. In most of the cases, the agreement between the theoretical and experimental values of the valence-band offsets is remarkably good. The accuracy of our theoretical values for the pure materials is on the order of 0.2 eV. Since we are looking at offsets here between ZnSe and $ZnS_xSe_{1-x}$ alloys with a maximum of only 26% S, the error bar for the pure materials will be reduced proportionally, to 0.05 eV. Considering this, the agreement between the theoretical and experimental values is fortuitously good (within 20 meV). More importantly, the trends in the data are correctly predicted. Regarding the results for conduction-band offsets, our calculated values are clearly much smaller than the error bar. We conclude, that the conduction-band offset is very small, in agreement with experiment, and too small to attach any significance to the difference between a type-I or type-II lineup.

In the case of the sample with very thin layers (18 Å–24 Å; sample a), we find that if we treat this superlattice as free-standing, then the calculated value of the total shift of the band gap works out to be about 85 meV compared with the experimental value of 45 meV. However, we know, based on the strain configurations of the other superlattices studied (see Table III), that this superlattice is most probably not free-standing. As a rough order of magnitude, the strain in ZnSe layers is almost one-half of the free-standing case. In this case, the total shift of the band gap for sample a works out to be about 52 meV. Note that this value is still much larger than the experimental one. However, since the binding energy of a free exciton in bulk ZnSe is about 18 meV, corresponding to a Bohr radius of about 38 Å, one would expect that there will be a significant increase in this binding energy in a superlattice with 18-Å wells. To our knowledge, no theoretical description exists, to date, to describe the behavior of exciton binding energy in a ZnSe-$ZnS_xSe_{1-x}$ system with practically zero conduction-band offset.

Finally, for the case of the superlattice whose total thickness is about 1000 Å (sample c), we see that the measured strain in the ZnSe layers is negligibly small (Table III), confirming a pseudomorphic growth of this structure with the ZnSe buffer layer.

The experimental observations as well as the theoretical predictions described above indicated a very small conduction-band discontinuity. Since a larger barrier height for confinement of electrons would be useful for certain applications, one should explore whether other superlattice systems can provide a larger $\Delta E_c$ value. While it is difficult to perform an exhaustive search experimentally, our theoretical approach allows us to readily examine all possibilities, with the confidence instilled by the remarkably good agreement with experiment in the cases discussed. One easily finds that the valence-band discontinuity can be varied over quite a large range, especially if one increases the sulfur content of the $ZnS_xSe_{1-x}$ alloy. For a particular alloy composition, variation of the strain (by changing $a^{\parallel}$) has important

effects on $\Delta E_v$, mainly because of the sizable splitting caused by the uniaxial strain. $\Delta E_c$, on the other hand, will always remain very small. This is a consequence of the initially small separation of these levels in the unstrained material (see Table II), which is even decreased by appropriate inclusion of the strain effects necessary to obtain a pseudomorphic strained-layer interface. The (nondegenerate) conduction band is not subject to any uniaxial strain splittings, and the hydrostatic components of the strain will always drive this system in the direction of a very small conduction-band offset.

## VIII. CONCLUSIONS

We have clearly demonstrated the effects of strain and carrier confinement in ZnSe-$ZnS_xSe_{1-x}$ strained-layer superlattices. We have shown that for the case where the total thickness of the SLS is smaller than its critical thickness, the lattice constant of the superlattice is that of the buffer layer so that the ZnSe well layers are not under strain. In this case all the observed blue shift in the exciton energies is attributed to carrier confinement effects. The band offsets are still affected in this case because the $ZnS_xSe_{1-x}$ barrier layers are under tensile strain. For the case of the SLS whose total thickness is larger than its critical thickness, we found it necessary to include the strain effects in ZnSe wells also. Theoretical calculations of the band offsets, based on the model solid approach, agree with the experimental observations to better than the theoretical error bar of 0.05 eV. They indicate that all possible ZnSe-$ZnS_xSe_{1-x}$ interfaces will exhibit a very small conduction-band offset.

## ACKNOWLEDGMENTS

We would like to thank R. Dalby, D. A. Cammack, and H. Cornelissen for supplying the MBE samples, J. Petruzzello for providing the TEM data, and P. Newbury for taking the PL data. We would also like to thank Professor M. Cardona for several helpful discussions regarding the issue of band offsets.

*Formerly called Khalid Mohammed.

[1]G. C. Osbourn, IEEE J. Quantum Electron. **QE-22**, 1677 (1986); R. People, *ibid.* **QE-22**, 1696 (1986).

[2]J. E. Potts, T. L. Smith, and H. Cheng, Appl. Phys. Lett. **50**, 7 (1987); D A. Cammack, R. J. Dalby, H. J. Cornelissen, and J. Khurgin, J. Appl. Phys. Lett. **62**, 3071 (1987).

[3]T. Yokogawa, M. Ogura, and T. Kajiwara, Appl. Phys. Lett. **49**, 1702 (1986).

[4]S. Fujita, Y. Matsuda, and A. Sasaki, Appl. Phys. Lett. **47**, 955 (1985).

[5]K. Mohammed, D. J. Olego, P. Newbury, D. A. Cammack, R. Dalby, and H. Cornelissen, Appl. Phys. Lett. **50**, 1820 (1987).

[6]C. G. Van de Walle and R. M. Martin, Phys. Rev. B **34**, 5621 (1986).

[7]K. Mohammed, D. A. Cammack, R. Dalby, P. Newbury, B. L. Greenberg, J. Petruzzello, and R. N. Bhargava, Appl. Phys. Lett. **50**, 1820 (1987); J. Petruzzello, B. L. Greenberg, D. Cammack, and R. Dalby, J. Appl. Phys. **63**, 2299 (1988).

[8]J. W. Matthews and Blakeslee, J. Cryst. Growth **27**, 118 (1974).

[9]R. People and J. C. Bean, Appl. Phys. Lett. **47**, 322 (1985).

[10]O. Brafman, I. F. Chang, G. Lengyel, S. S. Mitra, and E. Carnall, Phys. Rev. Lett. **19**, 1120 (1967).

[11]G. E. Pikus and G. L. Bir, Fiz. Tverd. Tela **1**, 1642 (1959) [Sov. Phys.—Solid State **1**, 1502 (1959)].

[12]J. C. Hensel and G. Feher, Phys. Rev. **129**, 1041 (1963).

[13]G. Bastard, Phys. Rev. B **24**, 5693 (1981).

[14]P. J. Dean, D. C. Herbert, C. J. Werkhoven, B. J. Fitzpatrick, and R. N. Bhargava, Phys. Rev. B **23**, 4888 (1981).

[15]See, for example, J. Y. Marizn, M. N. Charasse, and B. Sermage, Phys. Rev. B **31**, 8298 (1985).

[16]C. G. Van de Walle and R. M. Martin, Phys. Rev. B **35**, 8154 (1987).

[17]C. G. Van de Walle and R. M. Martin, J. Vac. Sci. Technol. B **4**, 1055 (1986); C. G. Van de Walle (unpublished).

[18]W. A. Harrison, *Electronic Structure and the Properties of Solids* (Freeman, San Francisco, 1980), p. 253.

[19]D. Berlincourt, H. Jaffe, and L. R. Shiozawa, Phys. Rev. **129**, 1009 (1963).

[20]R. B. Hall and J. D. Meakin, Thin Solid Films **63**, 203 (1979).

[21]D. T. Marple, J. Appl. Phys. **35**, 1879 (1964).

[22]S. J. Czyzak, W. M. Baker, R. C. Crane, and J. B. Have, J. Opt. Soc. Am. **3**, 240 (1957); T. M. Biemewski, and S. J. Czyzak, *ibid.* **53**, 496 (1963).

[23]S. Shionoya, in *Luminescence in Inorganic Solids,* edited by P. Golgberg (Academic, New York, 1966), p. 205.

[24]Y. F. Tsay, S. S. Mitra, and B. Bendow, Phys. Rev. B **10**, 1476 (1974).

[25]D. W. Langer, R. N. Euwema, K. Era, and T. Koda, Phys. Rev. B **2**, 4005 (1970).